Shot-noise-limited control-loop noise in an interferometer with multiple degrees of freedom

Kentaro Somiya[1,2,*] and Osamu Miyakawa[3]

[1]Theoretical Astrophysics, California Institute of Technology, Pasadena, California 91125, USA

[2]Waseda Institute for Advanced Study, 1-6-1 Nishi-Waseda, Shinjuku, Tokyo 169-8050, Japan

[3]Institute for Cosmic Ray Research, The University of Tokyo, Chiba 277-8582, Japan

*Corresponding author: somiya@caltech.edu

Received 8 January 2010; revised 18 June 2010; accepted 7 July 2010;
posted 8 July 2010 (Doc. ID 122401); published 4 August 2010

Precise measurements, such as those made with interferometric gravitational-wave detectors, require the measurement device to be properly controlled so that the sensitivity can be as high as possible. Mirrors in the interferometer are to be located at specific operation points to isolate laser noise and to accumulate the signal in resonant cavities. On the other hand, rigid control of an auxiliary degree of freedom may result in imposing sensing noise of the control on the target object as excess force noise. Evaluation of this so-called *loop noise* is important in order to design a decent control scheme of the measurement device. In this paper, we show the method to calculate the level of loop noise, which has been recently implemented in simulation tools that are broadly used for designing gravitational-wave detectors. © 2010 Optical Society of America

OCIS codes: 040.0040, 120.0120, 140.0140.

1. Introduction

An interferometric gravitational-wave detector can measure a tiny change of the distance between two test masses a few kilometers apart by circulating the light in an optical resonator and also by separating the differential signal from common-mode laser noise [1–4]. It is just one degree of freedom, namely, the differential motion of the mirrors in the two long optical resonators, that is used to detect gravitational waves, while there are other degrees of freedom to be controlled so that the interferometer is set properly in its desirable operating point. Development of a decent control scheme is one of the issues in such a complicated device and in order to do so, we need a method to compare different control schemes in a quantitative way. Although the robustness, simplicity, and other practical issues can also be important, we focus on the noise coupling through the control loop, which could degrade the sensitivity.

Figure 1 shows our measurement device; a second-generation gravitational-wave detector that contains long optical resonators (arm cavities) and two recycling cavities in a Michelson interferometer. Gravitational waves will alter the differential length $L_- = L_1 - L_2$ between the input test masses (ITMs) and the end test masses (ETMs) that form the two arm cavities. There are four other degrees of freedom: the common motion of the arm cavities, $L_+ = L_1 + L_2$; the average distance between the power-recycling mirror (PRM) and the two ITMs, ℓ_p; the average distance between the signal-recycling mirror (SRM) and the two ITMs, ℓ_s; and the difference of the distance between the beam splitter (BS) and the two ITMs, ℓ_m.

A control signal is obtained by taking the beat of two light fields at different frequencies. A mirror motion produces phase modulation on the probe light. A pair of RF sideband fields is used as a

0003-6935/10/234335-08$15.00/0

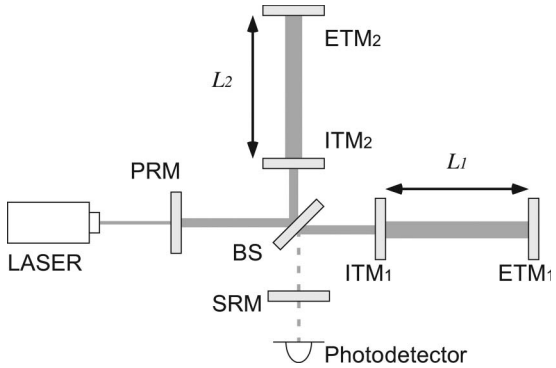

Fig. 1. Second-generation gravitational-wave detector.

reference that does not probe the mirror motion. Demodulating the beat by the sideband frequency, one can obtain the control signal. In a second-generation gravitational-wave detector, two or three weak sideband fields, besides the carrier field that probes the main signal, are injected into the interferometer. The light fields are picked off at various signal-extraction ports, each of which provides us with independent information of the five degrees of freedom to be controlled. Despite the efforts to obtain good signals using multiple fields and various ports, however, it is almost impossible to achieve the perfect separation of the signal since each field probes more than one degree of freedom to some extent, especially when one takes into account the imbalances of the arm cavities, which mix up the common-mode and differential-mode motions.

The level of loop noise is determined by two factors, the strength of the control signal and the separation of the signals. If the signal of a recycling cavity is obtained using the beat of the carrier field and the RF sidebands (single demodulation), the signal will not be well separated from the information of the arm cavities. If it is obtained from the beat of two pairs of RF sideband fields (double demodulation), the separation can be better, while the strength of the signal will not be as high as the single demodulation since the sideband fields are much weaker than the carrier. With the loop-noise calculation shown in this paper, one can quantitatively compare the single and double demodulations. This allows tuning parameters such as modulation depths or modulation frequencies of the sidebands to optimize the length-sensing and control scheme of the interferometer.

The purpose of this paper is not to make comparison of control schemes, which can be seen, for example, in Ref. [5], but to show the basic concept of the calculation and some related topics. The structure of the paper is as follows. In Section 2, we describe control noise in a general form. In Section 3, we show the loop noise of an interferometer, focusing on the first-order and the second-order contributions to obtain a naive but intuitive understanding. In Section 4, we formulate the loop-noise calculation including all kinds of cross talk of the control signals, and we explain gain reduction of the control signal caused by strong degeneracy. In Section 5, we demonstrate loop-noise calculation. In Section 6, we introduce a so-called feed-forward technique that can be used to lower the loop-noise level and a subeffect caused by the technique.

2. Generic Description of Feedback Control and Loop Noise

Any kind of measurement device imposes excess noise during the process to convert a target degree of freedom to output information. A good measurement device yields high conversion factor (= measurement gain) H and/or low sensing noise N_s during the process (see Fig. 2). The sensitivity on this measurement to obtain the information of x, the target degree of freedom, is determined by the measurement gain H, sensing noise N_s, and excess fluctuation of the target N_x. The measurement may require feedback control to set the device in its proper operation point with servo gain G. In fact, the servo gain does not affect the sensitivity, as it suppresses or enhances the signal and noise simultaneously.

A complex measurement device that contains an auxiliary degree of freedom can impose excess noise of this additional degree of freedom (n_x in Fig. 2). While the cross talk α to the main signal could be small, the fluctuation of the auxiliary degree of freedom can be large enough to contaminate the sensitivity of this measurement. To avoid the *nonorthogonality* as much as possible is a key of a good measurement device.

Feedback control can be used to suppress n_x, but it imposes sensing noise n_s to the output y_{aux} and, thus, to the main signal Y. Sensing noise on the auxiliary degree of freedom is inversely proportional to its measurement gain h. Here the output Y is given as

$$Y = \frac{1}{1+GH}(Hx + HN_x + N_s) + \frac{\alpha H}{1+GH}(x_{\mathrm{aux}} + n_x - g y_{\mathrm{aux}}), \quad (1)$$

with

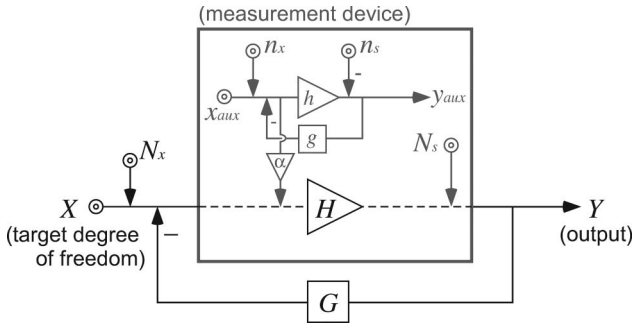

Fig. 2. Block diagram of a feedback control system with excess noise in the measurement device.

$$y_{\mathrm{aux}} = \frac{h}{1+gh}(x_{\mathrm{aux}} + n_x) - \frac{n_s}{1+gh}. \qquad (2)$$

Let us assume that x contains the signal and x_{aux} is zero. Comparing the signal and the noise components, we obtain the noise level expressed in the same unit of the observable as

$$x_n = N_x + \frac{N_s}{H} + \underline{\alpha\left(\frac{n_x}{1+gh} + \frac{gh}{1+gh}\frac{n_s}{h}\right)}. \qquad (3)$$

Each noise term is independent, so the sensitivity is given by taking the square sum of these terms. The underlined part is excess noise from the measurement device imposed due to the nonorthogonality of the system, which we called *loop noise*. It is actually only the second term of the part that appears with the nonzero open-loop gain gh, but let us extend the definition of loop noise to these two terms together for future discussion; especially for a related issue on a feed-forward technique that we show in Section 6. Equation (3) tells us that loop noise is αn_x when $gh \ll 1$, while it is $\alpha n_s/h$ when $gh \gg 1$. To decrease loop noise, we should decrease α and/or increase h. The open-loop gain gh should be properly chosen according to the ratio of noise terms at each frequency.

In this section, we introduced only the coupling from the auxiliary degree of freedom to the main signal, but there can be a coupling in the other direction, which results in reducing the gain H of the main signal. We will explain this *gain reduction* in Section 4.

3. Intuitive Understanding of Loop Noise in an Interferometer

In this section, we discuss loop noise more concretely with an interferometric gravitational-wave detector as an example measurement device. Figure 3 shows a part of the interferometer, including two pick-off ports inside and outside the power-recycling cavity. Signals obtained at the pick-off ports are fed back to the mirrors. These mirrors would be driven by seismic motion and thermal fluctuation, i.e., displacement noise, without the feedback control. In addition, sensing noise is imposed during the photodetection process, which includes quantum shot noise and photodetector noise. Once the feedback control is turned on, both displacement noise and sensing noise are suppressed in the control loop, but it does not necessarily mean that the mirror motion is suppressed. While the displacement-noise level can be lowered by the control, sensing noise on the feedback force drives the mirror. Even if classical displacement noise and detector noise is zero, shot noise that is converted to displacement noise remains in the presence of the control and would impose the ultimate limit of loop noise.

Because of degeneracy of the control signals, sensing noise of the auxiliary degrees of freedom appears in the main signal. The shot-noise level of ℓ_p, ℓ_m, or ℓ_s expressed in displacement is worse than that of L_-, since the circulating power in the recycling cavities is much lower than the power inside the arm cavities. The shot-noise level expressed in displacement, or the shot-noise-limited sensitivity, is inversely proportional to the optical gain of the target degree of freedom; thus, the circulating power is one of the important factors.

Since loop noise is imposed via control, the control bandwidth should be as narrow as possible. In a second-generation gravitational-wave detector, the lower end of the observation band is about 10 Hz and the control bandwidth is to be 10–50 Hz (this is indeed a consequence of the loop-noise calculation). Even if the control bandwidth can be set lower than the observation band, the slope of the low-path-filtered open-loop gain in the frequency domain cannot be too steep around the higher end of the control band, the unity-gain frequency, to avoid the system turning unstable. Thus, loop noise cannot be cut off immediately above the unity-gain frequency and it can easily limit the sensitivity.

Figure 4 shows a schematic of a normalized length-sensing matrix, which has been broadly used to express the signal separation at a certain frequency [6,7]. Each off-diagonal element means the ratio of the optical gain from a nontarget degree of freedom to the target degree of freedom in each signal-extraction port. Suppose that there are three nonzero off-diagonal terms; one is the ℓ_m motion mixed in the L_- signal, which is nonzero as far as some fraction of the carrier light is reflected by the ITMs without entering the arm cavities, and the others

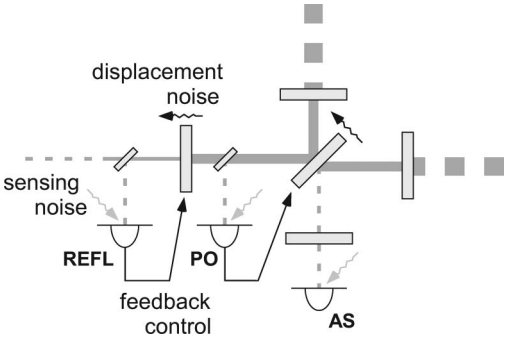

Fig. 3. Schematic of the feedback control in an interferometric gravitational-wave detector.

	$L+$	$L-$	lp	lm	ls
$L+$ port	1				
$L-$ port		1			
lp port			1		
lm port				1	
ls port					1

Fig. 4. First-order and second-order contributions of loop noise described in the normalized sensing matrix.

are the ℓ_p and ℓ_s motions mixed in the ℓ_m signal, which could be zero or large numbers, depending on the signal-extraction scheme. Shot noise of the ℓ_m drives mirrors in the control band and some fraction of the motion appears as noise in the L_- signal. This can be regarded as the first-order contribution of loop noise. In addition to the first-order, shot noise of ℓ_p and ℓ_s drives mirrors and some fraction of the motion appears as the ℓ_m motion, which, in turn, mixes into the L_- signal. This can be regarded as the second-order contribution [8].

While the first-order and the second-order could explain most of the part of loop noise in the case with a well-isolated signal-sensing scheme, a complete model is necessary to compare the single demodulation and the double demodulation, etc., and to explain the gain reduction due to the signal-sensing degeneracy. We shall systematically formulate the loop-noise calculation in Section 4.

4. Formulation of the Loop-Noise Calculation

Let us define the sensing matrix of our measurement device $\mathcal{D}$. Figure 5 shows a block diagram of a control system of the jth degree of freedom with some mixture from other degrees of freedom. The 5×5 matrix $\mathcal{D}$ converts the displacement vector $\mathbf{x}$ into the output vector $\mathbf{y}$, the elements of which are x_j and y_j and the indices $j = 1, 2, 3, 4, 5$ correspond to L_+, L_-, ℓ_p, ℓ_m, and ℓ_s, respectively. Sensing noise that is imposed on the measurement of each degree of freedom is represented by $\mathbf{n}$, as well.

In the absence of the feedback control, the output vector is given by

$$\mathbf{y} = \mathcal{D}\mathbf{x} + \mathbf{n}, \tag{4}$$

and from the measured output $\mathbf{y}$, the displacement information can be calibrated:

$$\mathbf{x}^{\mathrm{cal}} = \mathcal{D}^{-1}\,\mathbf{y} = \mathbf{x} + \mathcal{D}^{-1}\,\mathbf{n}. \tag{5}$$

The gravitational-wave signal appears mainly in x_2, so the signal-to-noise ratio in the second line of $\mathbf{x}^{\mathrm{cal}}$ would be the one to be considered [9,10]. In fact, we usually use only the y_2 term at the calibration process for simplicity. Thus, the calibrated displacement becomes

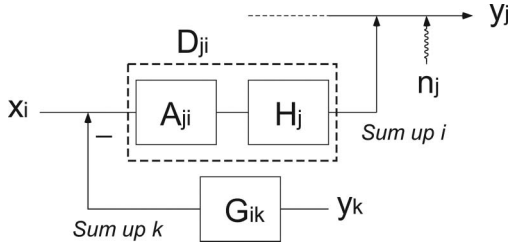

Fig. 5. Block diagram that shows the mixture of sensing noise and displacement noise of other degrees of freedom into each output. Here G_{ik} is the electric feedback-gain matrix element that sends y_k into x_i, and D_{ji} is the sensing matrix element that expresses the coupling from x_i into y_j. We split D_{ji} into the optical gain H_j and the normalized matrix element A_{ji}.

$$\tilde{x}_2^{\mathrm{cal}} = y_2/H_2 = x_2 + \sum_{j\neq 2} A_{2j}x_j + n_2/H_2, \tag{6}$$

where we define the optical-gain vector $\mathbf{H}$ by $H_j \equiv \mathcal{D}_{jj}$ and the normalized sensing matrix $\mathcal{A}$ by $A_{ji} \equiv D_{ji}/H_j$. On the right-hand side of Eq. (6), the first term represents the displacement information of L_- (i.e., gravitational-wave signal + displacement noise), the second term is displacement noise of the auxiliary degrees of freedom, and the third term is sensing noise on L_-.

Let us now turn on the servo control. In Fig. 5, $\mathcal{G}$ is the feedback-gain matrix. Not only displacement noise, but also sensing noise of the auxiliary degrees of freedom, can mix into the main output through the off-diagonal terms of $\mathcal{D}$ and $\mathcal{G}$. The output of the interferometer is given as

$$\mathbf{y} = -\mathcal{D}\mathcal{G}\mathbf{y} + \mathcal{D}\mathbf{x} + \mathbf{n}, \tag{7}$$

$$\rightarrow \mathbf{y} = (\mathcal{I} + \mathcal{D}\mathcal{G})^{-1}(\mathcal{D}\mathbf{x} + \mathbf{n}). \tag{8}$$

As we did in the case without the control, the y_2 component shall be considered. The x_2 component from Eq. (8) is taken as the gravitational-wave signal (plus displacement noise of L_-); the other x_j terms are extra displacement noise, and the square sum of all the n_j components is sensing noise. If $\mathcal{D}\mathcal{G}$ were perfectly diagonal, the matrix $(\mathcal{I} + \mathcal{D}\mathcal{G})^{-1}$ would have nothing to do with the signal-to-noise ratio, which would be just like the one obtained from Eq. (5), but it cannot be perfectly diagonal indeed and the nondiagonal matrix $\mathcal{D}\mathcal{G}$ plays an important role in generating loop noise. We will have discussions about the diagonalization in Section 6.

Suppose $\mathcal{G}$ is diagonal. We can approximate $(\mathcal{I} + \mathcal{D}\mathcal{G})^{-1} \simeq (\mathcal{D}\mathcal{G})^{-1}$ when the open-loop gains are sufficiently high. The second row of Eq. (8) then becomes

$$y_2 = \sum_j \frac{x_2 + A_{2j}^{-1} n_j/H_j}{G_{22}}, \tag{9}$$

which gives the loop-noise level in the unit of displacement as

$$x_{\mathrm{loop}} = \sum_{j\neq 2} A_{2j}^{-1} n_j/H_j. \tag{10}$$

Displacement noise of the auxiliary degrees of freedom appears to be zero. It represents the fact that the feedback control suppresses these motions. On the other hand, sensing noise of the auxiliary degrees of freedom couples to x_{loop} through the inverse matrix $\mathcal{A}^{-1}$. Determinant of $\mathcal{A}$ appears in the denominator on the right-hand side of Eq. (10), as if the optical gain becomes smaller than H_j. This gain reduction is what we did not see by the simple argument with the first- and second-order contributions in Section 3.

Let us show a simple example. Suppose there is a coupling of ℓ_m in L_-, represented by a, the

differential-mode and the common-mode controls of the recycling cavities are nonorthogonal by b, and the common-mode controls are significantly nonorthogonal by $1-\epsilon$, where a, b, $\epsilon \ll 1$; this is a typical situation in a second-generation gravitational-wave detector. The sensing matrix may be given as

$$\mathcal{A} = \begin{pmatrix} 1 & 0 & 0 & 0 & 0 \\ 0 & 1 & 0 & a & 0 \\ 0 & 0 & 1 & b & 1+\epsilon \\ 0 & 0 & b & 1 & b \\ 0 & 0 & 1-\epsilon & b & 1 \end{pmatrix}. \tag{11}$$

The inverse matrix of $\mathcal{A}$ is, approximately,

$$\mathcal{A}^{-1} \simeq \begin{pmatrix} 1 & 0 & 0 & 0 & 0 \\ 0 & 1 & ab/\epsilon & -a & -ab/\epsilon \\ 0 & 0 & 1/\epsilon^2 & b/\epsilon & -1/\epsilon^2 \\ 0 & 0 & -b/\epsilon & 1 & b/\epsilon \\ 0 & 0 & -1/\epsilon^2 & b & 1/\epsilon^2 \end{pmatrix}, \tag{12}$$

and the sensitivity becomes

$$\begin{aligned} x_{\mathrm{sens}} &= x_{\mathrm{shot}} + x_{\mathrm{loop}} \\ &= \frac{n_2}{H_2} + \frac{ab}{\epsilon}\left(\frac{n_3}{H_3}\right) - a\left(\frac{n_4}{H_4}\right) - \frac{ab}{\epsilon}\left(\frac{n_5}{H_5}\right). \end{aligned} \tag{13}$$

One can see the couplings from ℓ_p and ℓ_s have increased according to the gain reduction by the nonorthogonality factor ϵ.

5. Implementation

The concept of the loop-noise calculation is very simple, as we have seen. The calculation of the optical-gain matrix $\mathcal{D}$, on the other hand, is quite complicated to be done analytically, but there are a couple of frequency-domain simulation codes that we can rely on for this kind of matter [11,12]. One can obtain the optical-gain matrix using one of the codes, set up an appropriate feedback-gain matrix, and then implement them into Eq. (8) to get a loop-noise spectrum. There have been a number of loop-noise calculators based on our model [13–15]. Here we use our latest program written for a second-generation gravitational-wave detector [16]. The optical gain is calculated with the simulation software Optickle [12].

Figure 6 shows two tables, each of which is the normalized sensing matrix and the optical gain of the detector with a different signal-extraction scheme. The carrier light enters the arm cavities and returns to the reflection port (REFL). One of the phase-modulated sideband fields f_1 transmits through the central recycling cavities and goes to the antisymmetric port (AS). The other pair of phase-modulated sideband fields f_2 enters the power-recycling cavity and comes back to the reflection port. Reasonable imbalances in the arms and imperfections of the mirrors are included in the calculation. In Fig. 6(a), case (i), ℓ_p and ℓ_s are obtained with single demodulation. The error signals for L_+ and these two signals obtained from either the reflection port or a pick-off port in the power-recycling cavity (PO) are similar but still different [5]. The off-diagonal terms A_{31}, A_{32}, A_{51}, A_{52}, and A_{53} are not small. In Fig. 6(b), case (ii), ℓ_p and ℓ_s are obtained with double demodulation. The error signals are reasonably separated. Each element of the sensing matrix is a complex number. The number shown at the center is the absolute value of each element and the number on the shoulder is the argument; for example, in Fig. 6(b), the relative phases of A_{35} and A_{53} are different by 180° so ℓ_p and ℓ_s are not degenerated. While the matrices show a better signal separation with double demodulation, the optical gain is lower than that with single demodulation. We cannot simply say which case is the better one from these matrices. Therefore, we need to compute the loop-noise spectra.

Figure 7 shows the loop-noise spectra. Here the control bandwidth of the recycling cavities is set to 50 Hz, the servo gain decreases simply by $1/f$, and displacement noise of a recycling cavity is at the same level as the arm cavities. Figure 7(a) corresponds to case (i) and Fig. 7(b) to case (ii). Comparing the two cases, now we can see case (i), with the poorer signal separation and the higher optical gain, is better than case (ii). In fact, case (i) turns out to be the best of various possible signal-extraction schemes for this detector. Loop noise in either case contaminates the sensitivity in the observation band, unless we use a so-called feed-forward technique to reduce the effective noise coupling from other degrees of freedom to L_-, which will be explained in Section 6.

Our code to calculate loop noise has been implemented in the simulation tools for the second-

SDM+DDM	L_+	L_-	l_p	l_m	l_s	norm.
REFL f_2	1	1.4e-2 $^{-38}$	1.5e-2 ^{86}	3.8e-5 $^{-91}$	6.9e-7 $^{-94}$	4.9e18
AS DC	2.5e-4 ^{94}	1	9.8e-6 ^{169}	1.0e-3 $^{-9}$	3.4e-5 $^{-33}$	1.1e20
PO f_2	4.6e+0 ^{91}	3.9e+1 $^{-33}$	1	2.7e-2 $^{-89}$	1.8e-3 $^{-87}$	2.4e16
AS DDM	1.3e-3 $^{-22}$	1.9e-1 ^{132}	9.2e-1 ^{0}	1	1.2e-2 $^{-174}$	3.8e15
PO f_1	3.7e+1 ^{91}	3.3e+2 $^{-27}$	5.3e+0 ^{1}	2.0e-1 $^{-84}$	1	2.4e15

(a)

all DDM	L_+	L_-	l_p	l_m	l_s	norm.
REFL f_2	1	1.4e-2 $^{-38}$	1.5e-2 ^{86}	3.8e-5 $^{-91}$	6.9e-7 $^{-94}$	4.9e18
AS DC	2.5e-4 ^{94}	1	9.8e-6 ^{169}	1.0e-3 $^{-9}$	3.4e-5 $^{-33}$	1.1e20
REFL DDM	6.0e+0 ^{90}	2.2e-3 $^{-34}$	1	1.2e-2 ^{180}	3.5e-1 ^{180}	1.6e16
AS DDM	1.3e-3 $^{-22}$	1.9e-1 ^{132}	9.2e-1 ^{0}	1	1.2e-2 $^{-174}$	3.8e15
PO DDM	1.1e+1 ^{89}	1.2e+0 $^{-14}$	1.8e+0 ^{0}	3.6e-2 $^{-179}$	1	1.4e14

(b)

Fig. 6. Normalized sensing matrix $\mathcal{A}$ and the optical-gain vector $\mathbf{H}$ (i.e., normalized factor) at 100 Hz in two different cases of signal sensing for a second-generation gravitational-wave detector: ℓ_p and ℓ_s signals are obtained with single demodulation in panel (a) and with double demodulation in panel (b). For the other degrees of freedom, the signal-extraction ports are the same for two cases: L_+ from the reflection port, L_- from the dark port with dc readout [17–20], and ℓ_m from the dark port with double demodulation. Panel (a) shows poorer signal separation for the common-mode signals but higher optical gains, while panel (b) is the other way around. A small number in the top-right corner of each segment indicates the relative phase.

generation detectors. First we developed the code for Advanced-LIGO [21], which has been refined by a number of people. A similar code is used for Advanced-Virgo [22]. It is planned, in Advanced-Virgo, to change the detuning phase dynamically with different input laser powers, for which loop-noise analysis is a key issue. We wrote a slightly new code for the Japanese second-generation detector LCGT [16]. Proper treatment for the feed-forward technique was made for the new code. For the calculation results shown in Figs. 6–8, we use the parameters for LCGT.

6. Feed-Forward and Displacement-Noise Coupling

So far we have considered the feedback-gain matrix $\mathcal{G}$ to be a diagonal matrix. When the open-loop gain is sufficiently high, Eq. (8) becomes

$$\mathbf{y} \simeq \mathcal{G}^{-1}\mathcal{D}^{-1}\mathbf{n} + \mathcal{G}^{-1}\mathbf{x}. \tag{14}$$

By choosing proper matrix $\mathcal{G}$, the matrix $\mathcal{G}^{-1}\mathcal{D}^{-1}$ could be diagonalized so that each signal is free from shot noise of the other degrees of freedom. This feed-forward technique has been already used in currently operated gravitational-wave detectors. One can drive the L_- motion according to the output fluctuation of the auxiliary degrees of freedom. Sensing noise coupled through the control loop can be canceled by this additional displacement on L_-. The suppression factor of loop noise in a current detector is as much as 30–60 dB and it can be even more, while we should note that it is challenging to keep such high cancellation for long time.

Suppose the matrix $\mathcal{G}^{-1}\mathcal{D}^{-1}$ is diagonalized (i.e., $\mathcal{D}\mathcal{G}$ is diagonalized). We have learned in Eq. (8) that this diagonalization will make the sensitivity just like that without feedback control, and Eq. (14) tells us that it is indeed true. Without the feedback control, all the mirrors are moving freely and the motion of the mirrors appear via $\mathcal{D}$ in the L_- as extra displacement noise. With the feedback control and feed-forward, L_- is driven by the same amount as the original displacement noise of the auxiliary degrees of freedom, while the mirrors are under control.

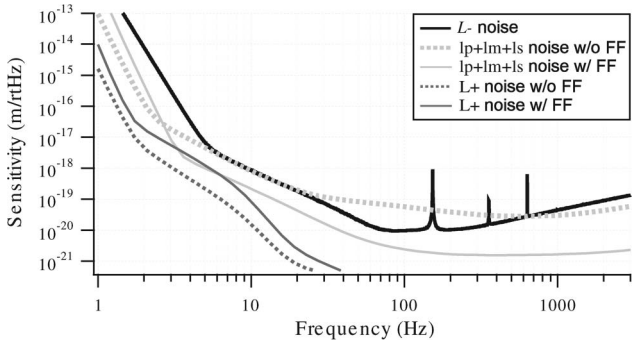

Fig. 8. Loop noise with and without feed-forward. With feed-forward, displacement noise at low frequencies and L_+ noise increase compared with the case without feed-forward.

In practice, we do not diagonalize $\mathcal{G}^{-1}\mathcal{D}^{-1}$, which requires too many feed-forward paths, but make the couplings from the recycling cavities to L_- zero by choosing proper G_{23}, G_{24}, and G_{25}. In the absence of other off-diagonal terms in $\mathcal{G}$, these feed-forward terms are given by the determinants of a 3×3 reduced inverse $\mathcal{D}$ matrix:

$$\overset{klm}{i} = \begin{pmatrix} D_{k3}^{-1} & D_{k4}^{-1} & D_{k5}^{-1} \\ D_{l3}^{-1} & D_{l4}^{-1} & D_{l5}^{-1} \\ D_{m3}^{-1} & D_{m4}^{-1} & D_{m5}^{-1} \end{pmatrix}, \tag{15}$$

as

$$G_{23} \to G_{33}\frac{\left|\overset{245}{i}\right|}{\left|\overset{345}{i}\right|} \simeq G_{33}\frac{D_{23}^{-1}}{D_{33}^{-1}}, \tag{16}$$

$$G_{24} \to -G_{44}\frac{\left|\overset{235}{i}\right|}{\left|\overset{345}{i}\right|} \simeq G_{44}\frac{D_{24}^{-1}}{D_{44}^{-1}}, \tag{17}$$

$$G_{25} \to G_{55}\frac{\left|\overset{234}{i}\right|}{\left|\overset{345}{i}\right|} \simeq G_{55}\frac{D_{25}^{-1}}{D_{55}^{-1}}. \tag{18}$$

In fact, according to the method used for feedback control in the gravitational-wave detector, there exist

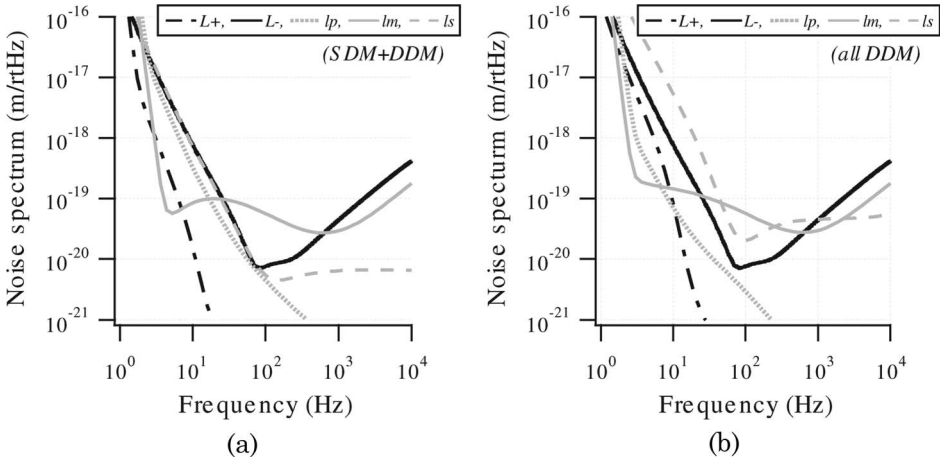

Fig. 7. Loop-noise curves of LCGT in the two cases introduced in Fig. 6 correspond to the matrix in (a) Fig. 6(a) and (b) Fig. 6(b).

a few nonzero off-diagonal terms in $\mathcal{G}$ before the feed-forward. We will discuss this *natural* cross talk in the feedback control in Appendix A.

Figure 8 shows the loop-noise level with and without the feed-forward. The sensing scheme and the setup are the same as that for the left panel of Fig. 7. The natural cross talk in $\mathcal{G}$ are not included. The feed-forward gains G_{23}, G_{24}, and G_{25} are the optimal ones with a $\pm 3\%$ error on each term, which corresponds to the $\sim$30 dB suppression (here we take a square average of eight combinations; $+3\%$ or -3% on G_{23}, G_{24}, or G_{25}). One can see that the feed-forward decreases loop noise from the recycling cavities at high frequencies, while it increases at low frequencies since displacement noise on the recycling cavities is imposed on L_-. This implies that the feed-forward should be turned off at low frequencies where the displacement-noise level is higher than the shot-noise level. One can also see that feed-forward increases L_+ loop noise, which is equivalent to frequency noise. This can be reduced by adding the appropriate G_{21} term, which is not in the plan of the current detector, but could be considered.

7. Summary

We presented the basic concept of loop noise, which is one of the important issues in a gravitational-wave detector. Degeneracy of the signal-sensing matrix of the device with multiple degrees of freedom causes the mixture of shot noise via control loops. We showed that the degeneracy also reduces the optical gain, which results in deterioration of the sensitivity. The loop-noise calculation tool let us compare different control schemes in terms of the noise level. Loop noise can limit the sensitivity of a gravitational-wave detector and the control scheme should be carefully chosen. The feed-forward technique is a way to reduce the contribution of loop noise, but it introduces displacement noise of auxiliary degrees of freedom to the main signal and also increases the frequency-noise coupling if we implement only the feed-forward for the recycling cavities.

Appendix A: Naturally Introduced Cross Talk in the Feedback Control

Here let us introduce two kinds of *natural* cross talk in $\mathcal{G}$. One is via the frequency stabilization loop; L_+ is fed back to the laser so that the laser frequency can be stabilized up to the level of tiny fluctuation of the long arm cavities. Changing the frequency influences the common-mode length measurements, that is, ℓ_p and ℓ_s. The off-diagonal terms G_{31} and G_{51} are given by G_{11} times the ratio from the recycling-cavity lengths to the arm length. The other kind is via the feedback control on the BS. Changing the BS position does not only change the differential mode ℓ_m, but also changes the recycling-cavity lengths. The off-diagonal terms G_{34} and G_{54} are given by $-G_{44}/2$ and $G_{44}/2$, respectively, unless we do feed-forward in the recycling cavities to resolve these couplings. The optimal feed-forward gains with this natural cross talk are given as

$$G_{23} \to G_{33} \frac{|_i^{245}| - F_2|_i^{124}|}{|_i^{345}| - F_1|_i^{145}| - F_2|_i^{134}|}, \tag{A1}$$

$$G_{24} \to -G_{44} \frac{|_i^{235}| + F_1|_i^{125}| - F_2|_i^{123}| - B_1|_i^{245}| - B_2|_i^{234}| - (F_1B_2 - F_2B_1)|_i^{124}|}{|_i^{345}| - F_1|_i^{145}| - F_2|_i^{134}|}, \tag{A2}$$

$$G_{25} \to G_{55} \frac{|_i^{234}| + F_1|_i^{124}|}{|_i^{345}| - F_1|_i^{145}| - F_2|_i^{134}|}. \tag{A3}$$

Here we defined $F_1 = G_{31}/G_{11}$, $F_2 = G_{51}/G_{11}$, $B_1 = G_{34}/G_{44}$, and $B_2 = G_{54}/G_{44}$. This natural cross talk increases loop noise by up to 30% in the case without the feed-forward. In the case with the feed-forward in G_{23}, G_{24}, and G_{25}, the difference can be a factor of 2 at some frequencies.

Most of the work shown in this paper was done in 2006 with the support of the Laser Interferometer Gravitational-Wave Observatory (LIGO) Visitors Program. We thank Peter Fritschel for inviting K. Somiya to the program and for valuable discussions. We also thank Rana Adhikari, Yoichi Aso, Stefan Ballmer, and Matt Evans for useful discussions. K. Somiya is currently supported by the Japan Society for the Promotion of Science (JSPS).

References and Notes

1. A. Abramovici, W. Althouse, R. Drever, Y. Gürsel, S. Kawamura, F. Raab, D. Shoemaker, L. Sievers, R. Spero, K. Thorne, R. Vogt, R. Weiss, S. Whitcomb, and M. Zucker, "LIGO: the Laser Interferometer Gravitational-Wave Observatory," Science **256**, 325–333 (1992).
2. C. Bradaschia, R. Del Fabbro, A. Di Virgilio, A. Giazotto, H. Kautzky, V. Montelatici, D. Passuello, A. Brillet, O. Cregut, P. Hello, C. Man, P. Manh, A. Marraud, D. Shoemaker, J. Vinet, F. Barone, L. Di Fiore, L. Milano, G. Russo, J. Aguirregabiria, H. Bel, J. Duruisseau, G. Le Denmat, Ph. Tourrenc, M. Capozzi, M. Longo, M. Lops, I. Pinto, G. Rotoli, T. Damour, S. Bonazzola, J. Marck, Y. Gourghoulon, L. Holloway, F. Fuligni, V. Iafolla, and G. Natale, "The VIRGO Project: a wide band antenna for gravitational wave detection," Nucl. Instrum. Methods Phys. Res. A **289**, 518–525 (1990).

3. H. Lück and the GEO600 Team, "The GEO600 project," Class. Quantum Grav. **14**, 1471–1476 (1997).
4. M. Ando and TAMA Collaboration, "Stable operation of a 300 m laser interferometer with sufficient sensitivity to detect gravitational-wave events within our galaxy," Phys. Rev. Lett. **86**, 3950–3954 (2001).
5. K. Somiya, P. Beyersdorf, K. Arai, S. Sato, S. Kawamura, O. Miyakawa, F. Kawazoe, S. Sakata, A. Sekido, and N. Mio, "Development of a frequency-detuned interferometer as a prototype experiment for next-generation gravitational-wave detectors," Appl. Opt. **44**, 3179–3191 (2005).
6. J. Mason and P. Willems, "Signal extraction and optical design for an advanced gravitational-wave interferometer," Appl. Opt. **42**, 1269–1282 (2003).
7. S. Sato, S. Kawamura, K. Kokeyama, F. Kawazoe, and K. Somiya, "Diagonalization of the length sensing matrix of a dual recycled laser interferometer gravitational wave antenna," Phys. Rev. D **75**, 082004 (2007).
8. K. Somiya, "Investigation of radiation pressure effect in a frequency-detuned interferometer and development of the readout scheme for a gravitational-wave detector," Ph.D. dissertation (University of Tokyo, 2004); Sec. 3.9.
9. It has been reported that ℓ_m contains more information of gravitational-wave signals at low frequencies in some configurations; see Ref. [10].
10. H. Rehbein, H. Müller-Ebhardt, K. Somiya, C. Li, R. Schnabel, K. Danzmann, and Y. Chen, "Local readout enhancement for detuned signal-recycling interferometers," Phys. Rev. D **76**, 062002 (2007).
11. A. Freise, "FINESSE," http://www.gwoptics.org/finesse/.
12. M. Evans, "Optickle," http://ilog.ligo-wa.caltech.edu:7285/advligo.
13. K. Somiya, "Length sensing and control of AdLIGO," presented at the LSC meeting, Baton Rouge, LIGO-G060481-00-Z (14–17 August 2006).
14. O. Miyakawa, "Calculation of loop noise for Advanced LIGO using Optickle engine," internal report (2006), http://lhocds.ligo-wa.caltech.edu:8000/advligo/Loopnoise results.
15. S. Ballmer, "Interferometer sensing and control," presented at the LSC meeting, Hannover, LIGO-G070687-00-I (22–25 October 2007).
16. http://gw.icrr.u-tokyo.ac.jp/JGWwiki/LCGT.
17. DC readout is a way to obtain the signal by adding an offset on the arm-cavity control and using the carrier light that leaks through the dark port as a reference; see Refs. [18–20]
18. K. Somiya, Y. Chen, S. Kawamura, and N. Mio, "Frequency noise and intensity noise of next-generation gravitational-wave detectors with RF/DC readout schemes," Phys. Rev. D **73**, 122005 (2006).
19. R. Ward, R. Adhikari, B. Abbott, R. Abbott, D. Barron, R. Bork, T. Fricke, V. Frolov, J. Heefner, A. Ivanov, O. Miyakawa, K. McKenzie, B. Slagmolen, M. Smith, R. Taylor, S. Vass, S. Waldman, and A. Weinstein, "dc readout experiment at the Caltech 40 m prototype interferometer," Class. Quantum Grav. **25**, 114030 (2008).
20. S. Hild, H. Grote, J. Degallaix, S. Chelkowski, K. Danzmann, A. Freise, M. Hewitson, J. Hough, H. Lück, M. Prijatelj, K. Strain, J. Smith, and B. Willke, "DC-readout of a signal-recycled gravitational wave detector," Class. Quantum Grav. **26**, 055012 (2009).
21. K. Somiya, O. Miyakawa, P. Fritschel, and R. Adhikari, "Length sensing and control for AdLIGO," Tech. Rep. LIGO-T060272-00-I (2006), https://dcc.ligo.org/
22. The Virgo Collaboration, "Advanced Virgo baseline design," VIR-027A-09 (2009), https://pub3.ego-gw.it/itf/tds/.